Thermal aging of fiberglass/carbon-fiber hybrid composites

E. Barjasteh*, E.J. Bosze, Y.I. Tsai, S.R. Nutt

1. Department of Chemical Engineering and Materials Science, University of Southern California, Los Angeles, CA 90089, United States
2. Composite Technology Corporation, Irvine, CA 92614, United States

Abstract:

Thermal oxidation of a unidirectional carbon-fiber/glass-fiber hybrid composite was investigated to determine oxidation kinetics and degradation mechanisms. The epoxy composite rods were comprised of a carbon-fiber core and a glass-fiber shell. A reaction–diffusion model was developed for each of the two hybrid sections to obtain the oxygen-concentration profile and the thickness of the oxidized layer (TOL) within the composite rods. The TOL was measured experimentally for samples exposed at 180 °C and 200 °C for up to 8736 h, and measured values were similar to the modeling predictions. The glass-fiber shell functioned as a protective layer, limiting the oxidation of carbon-fiber core. A relationship was derived relating TOL to tensile strength of the hybrid composite. The tensile strength remained essentially unchanged by thermal oxidation after 52 weeks of exposure. Inspection of thermally aged capped rods showed no cracking after long-term exposures.

Key words: A. Carbon-fiber; A. Glass-fiber; B. Environmental degradation; Thermal oxidation

1. Introduction

A relatively new application for polymer matrix composites involves the support of overhead conductors for power distribution. In this application, overhead power lines are supported by a unidirectional hybrid (carbon/glass-fiber) composite [1]. In contrast, traditional Al conductors are

Please cite this article as E. Barjasteh, E. Bosze, Y-I Tsai, and S.R. Nutt, "**Thermal aging of fiberglass/carbon fiber hybrid composites**" Composites A 40 [12] (2009) 2038-2045.
DOI<http://dx.doi.org/10.1016/j.compositesa.2009.09.015>

supported by steel cable, and this has been the case for the past 100 years. However, the recently developed composite-supported conductors, termed ACCC for aluminum conductor/composite core, present multiple advantages for economic and efficient transmission of electrical power [2]. In particular, the ACCC conductors exhibit greater strength, lower weight, and less sag at high temperatures.

Despite the considerable advantages in mechanical performance, long-term durability of composite conductors is a major concern, as overhead conductors are expected to retain properties with minimal maintenance over a service life that spans multiple decades. These concerns stem from the uncertain effects of long-term environmental exposure, which includes temperature, moisture, radiation, and aggressive chemicals, all of which can be exacerbated by cyclic loads. In general, the mechanical and physical properties of polymer composites are adversely affected by such environmental factors [3] and [4]. Consequently, the ability to forecast changes in material properties as a function of environmental exposure, particularly bulk mechanical properties, which are affected by the integrity of fiber–matrix interfaces, is required to design for extended service lives.

At high temperatures (approaching the glass transition temperature T_g), polymer composites are susceptible to oxidative degradation [5], [6], [7] and [8]. Although the fibers are stable at such temperatures (less than T_g), the matrix and especially the fiber–matrix interface can undergo degradation that affects the physical and mechanical properties of the structure over time. Matrix oxidation of composites has been investigated for polymers such as polybismaleimide [9] and [10] and amine cured epoxy [11], [12] and [13]. The oxidation is initially limited to a superficial layer until cracks appear in the layer. Cracks open new pathways for oxygen to penetrate the specimen

and lead to more extensive oxidation. This process can continue until the polymer is completely oxidized. During oxidation, polymers undergo mass loss, shrinkage, and density increase [14].

Oxidative degradation of the matrix of polymer composites generally resembles that of the neat polymer. However, the fibers and the fiber–matrix interface significantly alter the transport properties of oxygen, introduce anisotropy, and influence the extent of damage within the composite.

Oxidation-induced damage in unidirectional composites is typically manifest as matrix cracks [15] and [16]. Note that cracks initiate in the composites because of the stress gradient induced by shrinkage of the oxidized matrix [16], but are also depend on the properties of the fiber–matrix interface [17] and [18] and on fiber orientations [19]. In particular, oxidation-induced cracks in unidirectional composites often initiate at fiber tips exposed at surfaces. Furthermore, fiber orientation affects and sometimes determines the extent of cracking, particularly in directions parallel to the fiber orientation. Spontaneous cracks due to matrix oxidation initiate and propagate within the oxidized layer at the surface of the structure [16]. Therefore, prediction of the thickness of the oxidized layer, TOL, helps to design more efficient and durable structures and hence to prevent as much damage as possible.

The purpose of the present work was to determine kinetics of thermal oxidation and associated damage mechanisms for unidirectional hybrid composites designed to support overhead conductors. A coupled reaction–diffusion model was developed for the carbon-fiber (CF) core and the glass-fiber (GF) shell to predict the oxygen-concentration profile and the TOL. The effect of oxidation on tensile strength and on crack initiation and propagation in the hybrid composite was analyzed.

Finally, a relationship was derived to show the dependence of tensile strength on the ratio of TOL to thickness of sample (TS) for unidirectional hybrid composites.

2. Experiments

2.1 Materials and conditioning

Unidirectional hybrid composite rods were produced by pultrusion (Composite Technology Corporation, Irvine, CA). The rods were comprised of a carbon-fiber core (CF) surrounded by a glass-fiber shell (GF), as shown in Fig. 1. The epoxy matrix was designed to achieve a high glass-transition temperature (T_g) using a proprietary epoxy formulation and an anhydride curing agent. The rod characteristics are shown in Table 1. In addition, control samples were produced by a clear casting method that involved curing the neat resin for 1 h at 200 °C.

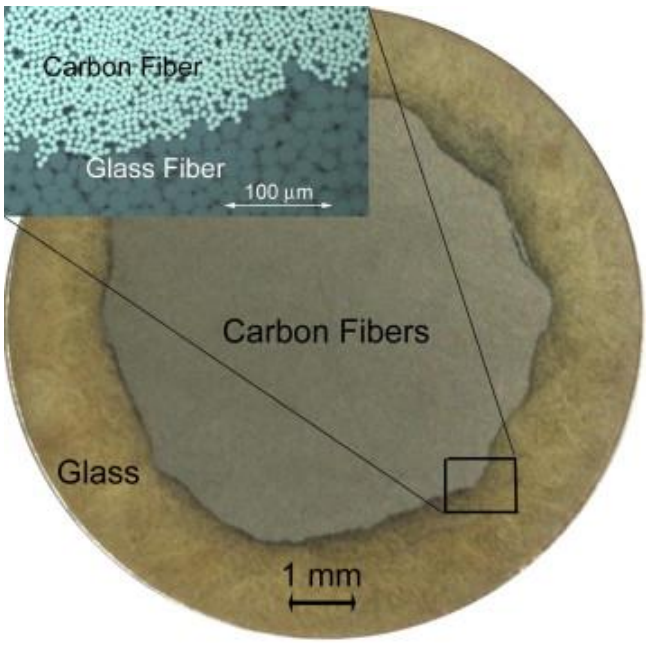

Fig. 1. Cross section of pultruded hybrid composite rod, showing the carbon core surrounded by the glass shell.

Table 1. Characteristics of carbon-fiber core and glass-fiber shell in hybrid composite rod.

	r_i(mm)	r_0(mm)	Glass volume (%)	Carbon volume (%)	Epoxy volume (%)	Cross-sectional area (%)
Carbon core	0	6.8	0	69	31	51
Glass shell	6.8	9.5	64	0	36	49

Sample composite rods (9.5-mm diameter) were placed in an air-circulated oven at 180 °C and 200 °C and 1-atmosphere pressure for isothermal aging. Samples were separated to allow convection, and sample ends were capped with a silicone sealant to prevent the end-diffusion of oxygen. The weight loss was recorded at intervals using an analytical balance (ACCULABLA-60) with 0.001 mg accuracy. Samples were cooled in a desiccator for 10 min before every measurement to prevent moisture adsorption. The same procedure was used for clear-cast samples to record weight loss.

2.2 Mechanical testing and thermal analysis

The mechanical and thermal properties of composite rods were measured after different thermal oxidation exposure. Dynamic mechanical analysis (DMA) was performed using a dual-cantilever-beam clamp (TA Instruments DMA2980) to measure the T_g values of oxidized composite rods and control samples of neat epoxy. DMA experiments were performed in accordance with standard protocol (ASTM D7028), and a ramp rate of 5 °C/min was used for all specimens. The peak in the loss modulus curve was taken as the T_g value for composite rod samples (normally ~225 °C).

The tensile strength of the composite core was measured using a computer-controlled load frame (Instron 5585) following ASTM Standard D3916. Composite core samples were mounted in the load

frame using adhesive gripping in custom-made fixtures. Tensile tests were performed by preloading the samples to 4.5 kN and holding for 5 min to allow load redistribution in the load train. The load was applied using a crosshead speed of 5 mm/min (0.2 in./min) until failure occurred. All tests were conducted at room temperature.

Oxygen-diffusivity measurements were performed on thin-film clear-cast samples using the half-time method [27] (Mocon Company, Minneapolis, MN). Table 2 shows the measured transport coefficients and oxygen solubility values for the hybrid composites. Note that D_1, the axial diffusivity parallel to the fiber direction, is calculated based on the Kondo relationship [20], $D_1 = (1 - V_f) \cdot D_2/(1–2 \cdot \sqrt{(V_f/\pi)})$, where V_f is the volume fraction of fibers. Note that D_2, the diffusivity in the transverse direction, is slightly lower than the diffusivity of the unreinforced epoxy. Oxygen solubility, *s*, is nearly independent of temperature. The surface concentration of oxygen was determined based on Henry's equation, $C_s = s \cdot P_{O2}$, where P_{O2} is the partial pressure of oxygen in ambient (lab air). Light microscopy of polished sections was used to measure the oxidized thickness of samples and to detect cracks.

Table 2.Values of oxygen diffusivity for the hybrid composite components, where axial and transverse diffusivity are represented by D_1 and D_2, and C_s is the surface concentration of oxygen.

Temperature (°K)	D glass shell ($m^2\ s^{-1}$)		D carbon core ($m^2\ s^{-1}$)		Solubility (10^{-4} mol $m^{-3}Pa^{-1}$)	C_s (mol m^{-3})
	$D_1(10^{-12})$	$D_2(10^{-12})$	$D_1(10^{-12})$	$D_2(10^{-12})$		
180	3.75	0.70	2.59	0.70	3.52	7.10
200	5.36	1.10	3.70	1.10	3.52	7.10

Nanoindentation measurements were performed on resin-mounted oxidized epoxy samples using a 100 nm Berkovich tip (TriboIndenter, Hysitron, Minneapolis, MN). Tests were carried out on samples isothermally aged at 200 °C for 820 h, 1600 h and 3200 h. The loading rate was 1000 μN/s, and the maximum load used for each test was 5000 μN. Twenty indents were performed for each

specimen with an indentation spacing of 10-μm. Standard nanoindentation drift correction measures were applied during the tests.

2.3 Modeling

The most appropriate model to describe the present system is a reaction–diffusion model that predicts the extent of oxidation and distribution of oxygen (concentration profile) within the hybrid composite. Oxygen molecules are assumed to diffuse into the composite and react with the epoxy matrix. Considering the geometry of the rod, the oxygen balance equation, Fick's second law, is written in cylindrical coordinates.

$$\frac{\partial \boldsymbol{C}}{\partial \boldsymbol{t}} = \boldsymbol{D}_{\boldsymbol{i}=\boldsymbol{r},\theta,\boldsymbol{z}}\left[\frac{1}{\boldsymbol{r}}\frac{\partial}{\partial \boldsymbol{r}}\left(\boldsymbol{r}\frac{\partial \boldsymbol{C}}{\partial \boldsymbol{r}}\right) + \frac{1}{\boldsymbol{r}^2}\frac{\partial^2 \boldsymbol{C}}{\partial \theta^2} + \frac{\partial^2 \boldsymbol{C}}{\partial z^2}\right] + \boldsymbol{R}(\boldsymbol{C}) - \boldsymbol{x}_{\mathrm{O}_2}\sum_{\beta=1}^{N}\boldsymbol{R}_{\beta} \tag{1}$$

where $\boldsymbol{C}$ is the oxygen concentration within the sample, $\boldsymbol{D}_r$, D_z and D_θ are the diffusion coefficients, $\boldsymbol{R}(\boldsymbol{C})$ is the consumption rate of oxygen, and $\boldsymbol{R}_\beta$ is the production rate of volatile β.

Several assumptions are made in constructing a model to simulate oxygen diffusion in the composite rod. Because the structure is essentially infinite in the axial ("z") direction and symmetrical in the θ direction, we assume that the molar mass transfer of oxygen is unidirectional and occurs in the transverse direction r (perpendicular to the fibers). Hence, the oxygen-concentration gradients in z and θ directions become zero, and the corresponding terms are eliminated from the balance equation. Furthermore, we neglect the effect of the transfer of gaseous volatiles. These volatiles

diffuse toward the surface of the composite rod, while oxygen diffuses in the opposite direction, toward the rod center. The geometry and dimensions of the model system are shown in Fig. 2.

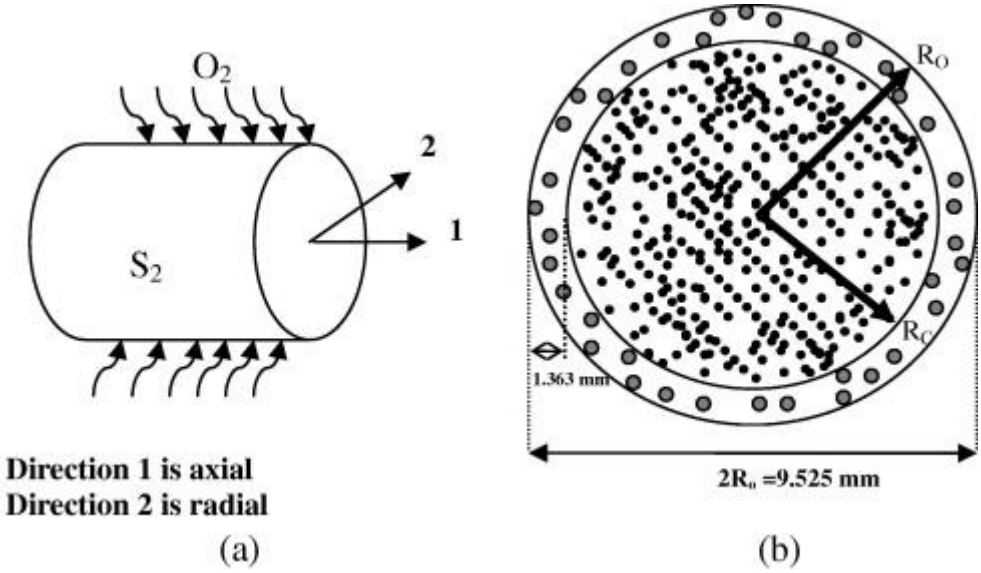

Fig. 2. (a) Schematic of composite rod with coordinates. The oxygen diffuses in the radial direction 2. (b) Transverse section of composite rod.

The mole balance equations for the shell and core of the hybrid composite, shown in Eqs.(2) and (3) are:

$$\frac{\partial C_g}{\partial t} = D_{glass/epoxy}\left(\frac{\partial^2 C_g}{\partial r^2} + \frac{1}{r}\frac{\partial C_g}{\partial r}\right) - R_1(C_g) \tag{2}$$

$$\frac{\partial C_c}{\partial t} = D_{Carbon/epoxy}\left(\frac{\partial^2 C_c}{\partial r^2} + \frac{1}{r}\frac{\partial C_c}{\partial r}\right) - R_2(C_c) \tag{3}$$

where $D_{\mathrm{glass/epoxy}}$ and $D_{\mathrm{Carbon/epoxy}}$ are the diffusivities of oxygen through the glass shell and carbon core, respectively. In these expressions, $\mathrm{R_1(C_g)}$ and $\mathrm{R_2(C_c)}$ are the reaction rates of oxygen within the glass shell and the carbon core, respectively. Initially, $C = 0$ for all points in the rod. The boundary conditions are:

$$r = R_o: \quad C_g = C_s; \tag{4}$$

$$r = R_c: \quad C_g = C_c; \tag{5}$$

$$\frac{\partial C_c}{\partial r} = \frac{\partial C_g}{\partial r}; \tag{6}$$

$$r = 0: \quad \frac{\partial C_c}{\partial r} = 0 \tag{7}$$

where C_s is the concentration of oxygen at the surface of composite rods.

Boundary conditions at $r = R_c$ are defined assuming a continuous oxygen concentration at the CF–GF core–shell interface. The matrix material in both components is a cyclo-aliphatic epoxy. However, the diffusion coefficients are not identical for the two sections. The difference stems from multiple factors, including the fact that the fiber volume fractions are not the same in the two sections, nor is the path length (tortuosity) [21] and [22]. In particular, the tortuosity, which is inversely related to diffusivity, differs in the two sections because of the different diameters of CF and GF [26].

The kinetic scheme of the polymer oxidation includes a series of chain radical reactions (Eqs. (8), (9), (10), (11), (12) and (13)). These reactions, which generate a self-initiator, are known as the closed loop standard mechanistic scheme [6]. The unimolecular decomposition of hydroperoxide is considered because of the high temperature exposure, and the scheme is shown below:

$$\mathrm{POOH} \rightarrow 2\mathrm{P}^{\circ} + \mathrm{H_2O} + \mathrm{vV} \qquad K_1 \tag{8}$$

$$\mathrm{P}^{\circ} + \mathrm{O_2} \rightarrow \mathrm{PO}_2^{\circ} \qquad K_2 \tag{9}$$

$$\mathrm{PO}_2^{\circ} + \mathrm{PH} \rightarrow \mathrm{POOH} + \mathrm{P}^{\circ} \qquad K_3 \tag{10}$$

$$\mathrm{P}^{\circ} + \mathrm{P}^{\circ} \rightarrow \text{inactive products} \qquad K_4 \tag{11}$$

$$P^{\circ} + PO_2^{\circ} \rightarrow \text{inactive products} \qquad K_5 \tag{12}$$

$$PO_2^{\circ} + PO_2^{\circ} \rightarrow \text{inactive products} + O_2 \qquad K_6 \tag{13}$$

where K_1–K_6 are the reaction rate constants.

In the kinetic scheme, only the oxygen reaction rate is heterogeneous, and oxygen availability depends on the diffusivity. The oxygen mole balance in cylindrical coordinates is given below.

$$\frac{\partial[O_2]}{\partial t} = D\left(\frac{\partial^2[O_2]}{\partial r^2} + \frac{1}{r}\frac{\partial[O_2]}{\partial r}\right) + k_2[O_2][P^{\circ}] - k_6[PO_2^{\circ}]^2 \tag{14}$$

The relation of O_2 consumption rate, $R(C)$, with oxygen concentration, C, can be derived by manipulating the differential equations generated from the kinetic scheme [9], yielding Equation (15):

$$\boldsymbol{R(C)} = 2\boldsymbol{r}_0 \frac{\beta[O_2]}{1+\beta[O_2]}\left[1 - \frac{\beta[O_2]}{2(1+\beta[O_2])}\right] \tag{15}$$

where $\boldsymbol{r}_0$, is the maximal oxidation rate in oxygen excess, and β is the reciprocal of the critical oxygen concentration beyond which oxygen excess is reached. These parameters are measured from the gravimetric curve presented in the following section.

Carbon fibers reportedly can have a stabilizing effect on thermal aging of composites [23]. At the fiber–matrix interface, the CF absorbs and deactivates radicals that would potentially react with diffusing oxygen molecules. The phenomena described here indicate the need for additional equations in the kinetic scheme. As a result, the reaction rate parameters, $\boldsymbol{r}_0$ and β, and consequently the expression for the oxidation reaction rate differ for the CF section and the GF section [23].

3. Results

3.1 Oxidation thickness

Fig. 3 shows the weight loss of the composite rods as a function of aging time, indicating that the weight loss increased with exposure time and temperature. The rate of weight loss was relatively high in the first 10–20 h, then appeared to reach a steady state for the duration of the aging.

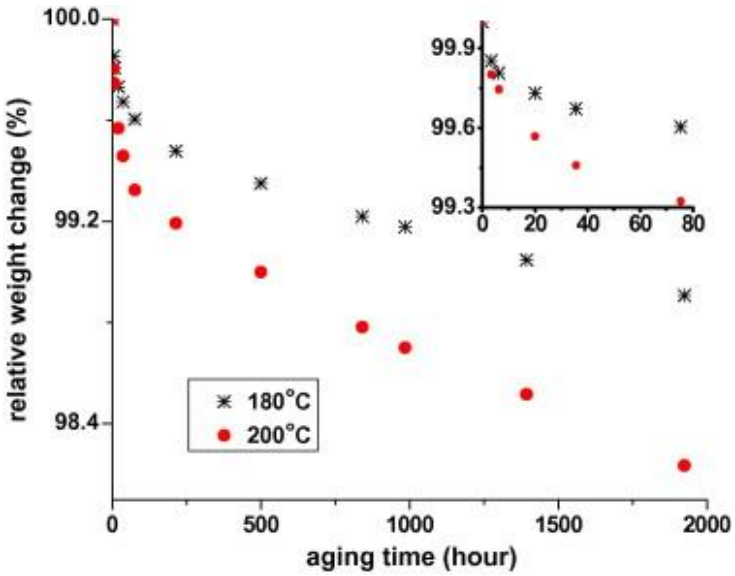

Fig. 3. The gravimetric curve obtained for capped composite rods 30.48 mm in length and 9.525 mm in diameter, thermally aged at 180 °C and 200 °C.

The total weight change of the hybrid composite is expressed in Eq. (16) [23]. The weight change resulted from (a) the loss of volatiles (V and μ_o), (b) water elimination from the structure, and (c) weight gain associated with the oxidation.

$$(1-w_f)\frac{1}{m_0}\frac{dm}{dt}=\frac{32}{\rho_0}R(C)-\frac{18}{\rho_0}\frac{d[H_2O]}{dt}-\frac{M_v}{\rho_0}\times\frac{d[V]}{dt}-\mu_o \quad (16)$$

where w_f, M_v, m, ρ_0 and μ_o are the mass fraction of fibers, average molar mass of volatile fragments, the mass of the specimen, initial density, and the volatile emission in the absence of oxygen, respectively. Volatile emission, μ_o, was measured from the gravimetric curve generated during the exposure of a thin-film specimen in pure nitrogen. Each term on the right side of Eq. (16) can be expressed in terms of oxygen concentration using kinetic equations, leading to a final equation relating the mass loss to the oxygen concentration [9].

Fig. 4 shows the weight-loss data of thin-film samples (30 μm) versus aging time for exposures at different partial pressures of oxygen (1-atmosphere total pressure) at 200 °C. The sample exposed in nitrogen (inert atmosphere) showed a lower rate of weight loss than those exposed in oxidizing atmospheres. The rate of weight loss increased with increasing oxygen content in the ambient, indicating that the weight loss resulted mainly from thermal oxidation. In other words, oxidation level is directly proportional to oxygen concentration. The weight-loss data were used to calculate the kinetic parameters, r_0 and β, for the oxidation of anhydride-cured epoxy, as shown in Table 3. These reaction rate parameters were adapted for the oxidation of CF–epoxy composites following accepted protocols [23].

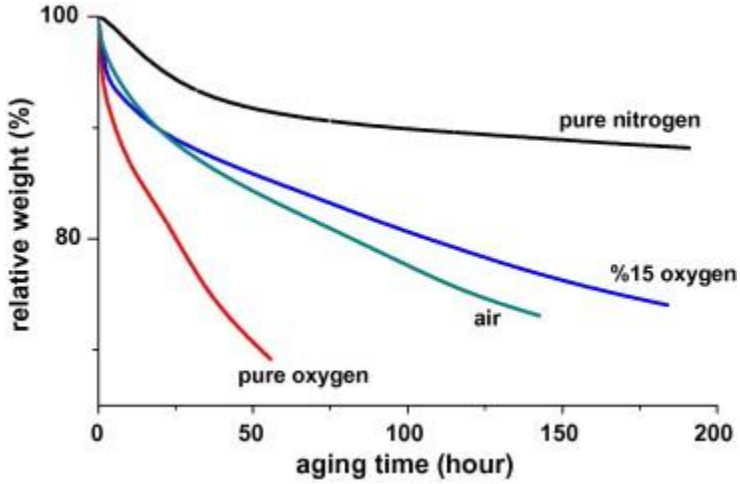

Fig. 4. Weight loss of samples (30 ± 5 μm thick) exposed to different partial pressures of oxygen at 200 °C.

Table 3. Reaction rate parameters, r_0 and β, obtained at 180 and 200 °C for the cycloalyaohatic anhydidride cured epoxy.

	Carbon section		Glass section	
Aging temperature (°C)	r_0 (10^{-3} s^{-1})	β (l $mole^{-1}$)	r_0 (10^{-3} s^{-1})	β (l $mole^{-1}$)
180	3.2	93.3	2.9	103.1
200	10.0	69.5	8.9	75

After the required phenomenological parameters were determined, the two coupled non-analytical differential equations (Eqs. (2) and (3)), were solved. These equations were non-analytical because the expression for the oxygen reaction was nonlinear. The equations were solved numerically by applying the boundary and initial conditions, yielding predicted oxygen-concentration profiles within the carbon core, $C_c(r, t)$, and within the glass shell, $C_g(r, t)$.

Fig. 5 shows the predicted oxygen-concentration profiles as a function of radial position within the hybrid composite for different aging times. The predicted oxygen concentration decreased with increasing depth in the GF shell, as expected, and approached zero at depths of 25–150 μm, depending on aging time. Note that the concentration profiles were essentially the same for aging

times of 672 and 100 h. The prediction is accurate for longer aging times (to be shown below), unless the composite surface undergoes severe damage, such as surface erosion or cracking.

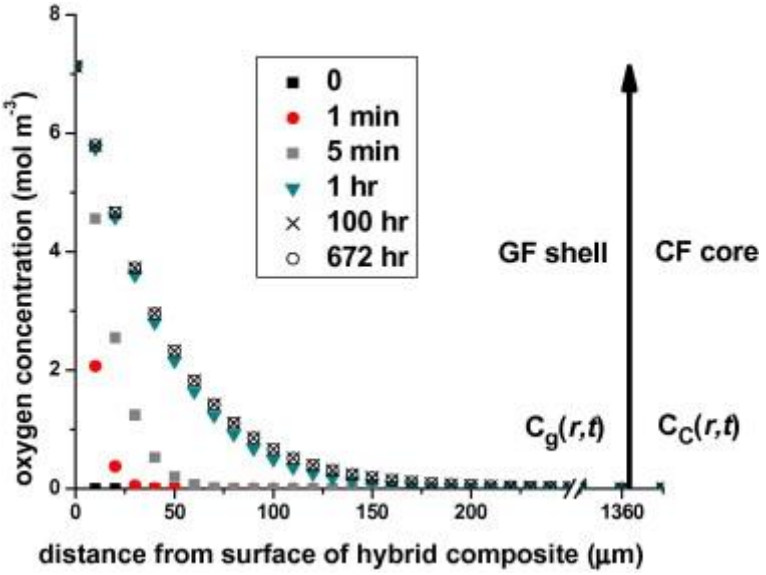

Fig. 5. Simulation prediction of oxygen-concentration profiles for hybrid composite rods, C_c (r, t) and C_g (r, t), in air at 180 °C.

Using Eq. (15), one can calculate the local oxygen consumption at a particular radial position by integrating the local oxygen-consumption rate over aging time, $Q = \int_0^t R(c) \cdot dt$. The calculated values can be used to plot the normalized oxygen consumption as a function of radial position within the hybrid composite. Such a plot is shown in Fig. 6 for different aging times. The plot indicates the amount of epoxy converted to oxidation product (conversion degree of oxidation). The oxygen consumption decreases with increasing subsurface depth and asymptotically approaches zero, because of the shortage of oxygen, as shown by the oxygen-concentration gradient (see Fig. 5). Thus, the oxidation thickness for different exposure times can be determined from the plot by simply reading the points at which the conversion degree is approximately zero. The oxidation-concentration profiles and associated reaction products formed relatively quickly (<100 h), and

thicknesses (TOL values) reached a limiting value of ~155 μm. The TOL remained essentially constant after 100 h, even for isothermal exposures up to 1 year.

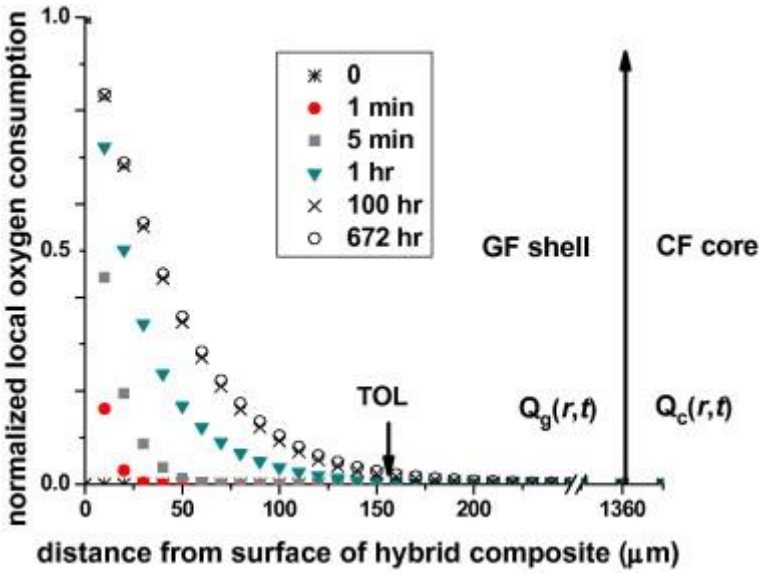

Fig. 6. Normalized oxygen consumption profiles predicted for hybrid composite rods, Q_c (r, t) and Q_g (r, t), in air at 180 °C.

The oxidation thickness was also measured by oxidizing rods (30.5 mm long) at 180 °C and 200 °C. Polished cross-sections of aged composite rods were inspected to measure the oxidization thickness (TOL), as shown in Fig. 7. The oxidation was limited to two discrete superficial layers within the GF shell. The outermost layer underwent more extensive oxidation, and was assumed to correspond to a 50% conversion of the matrix (see Fig. 6) [6]. The subsurface layer (*Y*), was less extensively oxidized, and the combined thickness of the two layers constituted the total oxidation layer of the composite, or TOL. Aging at 200 °C produced a TOL comprised of a single layer (two distinct layers were not detected). The measured TOL values for both aging exposure temperatures are tabulated in Table 4, along with model-based predictions. The thickness values were determined from the average of 20 thickness measurements at each temperature. Comparison of the measured and predicted TOL values reveals a difference of roughly 6%, both at 180 °C and 200 °C. Note that no

evidence of oxidation was detected within the CF core, which is consistent with the model-based calculation.

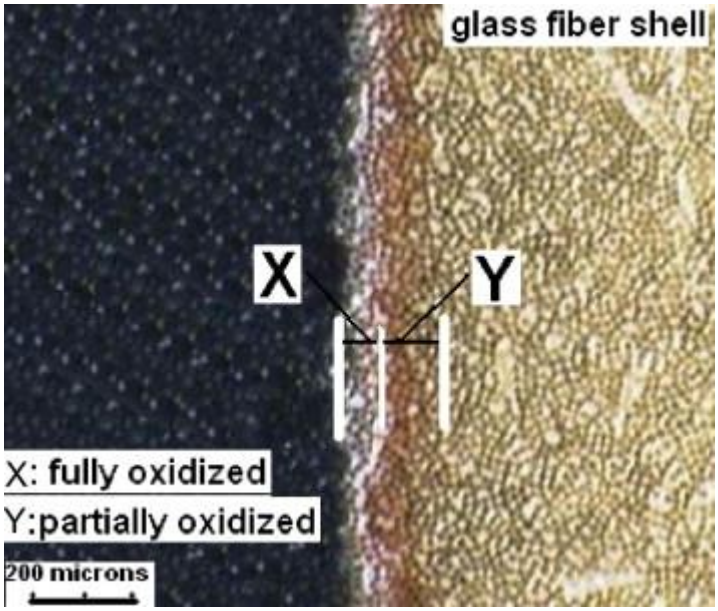

Fig. 7. Transverse cross section of hybrid composite rod thermally aged in air at 180 °C for 672 h. The TOLC is confined to a thin layer at the surface.

Table 4.Comparison of experimental measurement of TOLC with predicted values in air exposed for 672 h at different aging temperatures, 180 °C and 200 °C.

	Oxidation	Thickness (TOLC)
Temperature (°K)	Model prediction (μm)	Experimental measurement (μm)
180	155	146 ± 18
200	110	117 ± 5

Predictions of the TOL can be extended to longer aging times using the model presented here (Eqs. (2) and (3)). To illustrate, transverse cross-sections of composite samples aged for 8736 h (52 weeks) at 180 °C and 200 °C are shown in Fig. 9a and b, respectively. Inspection of the oxidized composite rods showed no significant changes in TOL, even after 52 weeks of aging. This is illustrated in Fig. 8, which shows the measured TOL values for thermal exposure at 180 °C. The plot also shows the predicted TOL value of 155 μm, which is similar to the measured TOL (~140 μm).

(Note that 180 °C is the maximum anticipated service temperature for the overhead conductors.) No evidence of crack initiation or propagation was detected, as described in the next section.

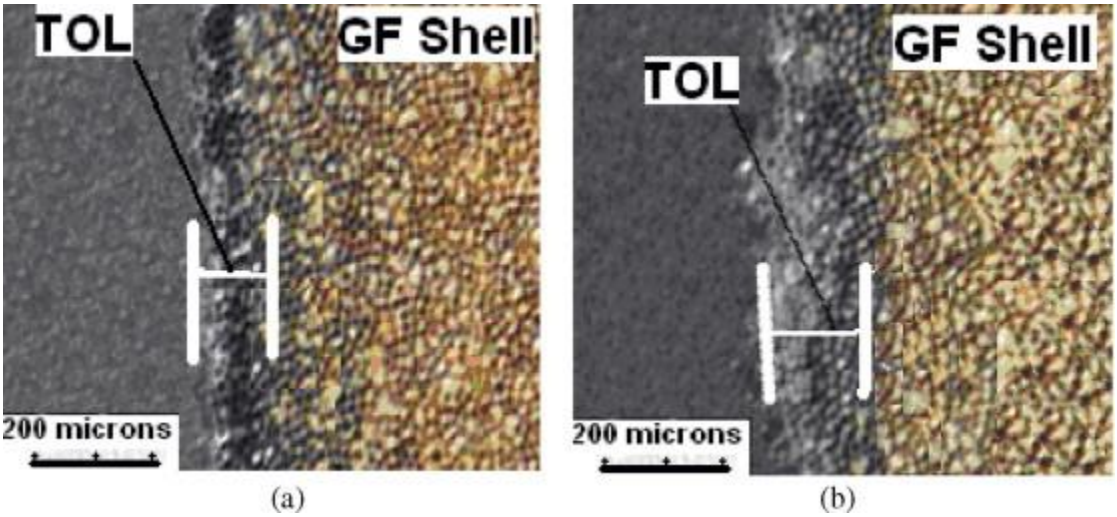

Fig. 9. Transverse cross section of hybrid composite rods thermally aged in air at (a) 180 °C and (b) 200 °C for 8736 h.

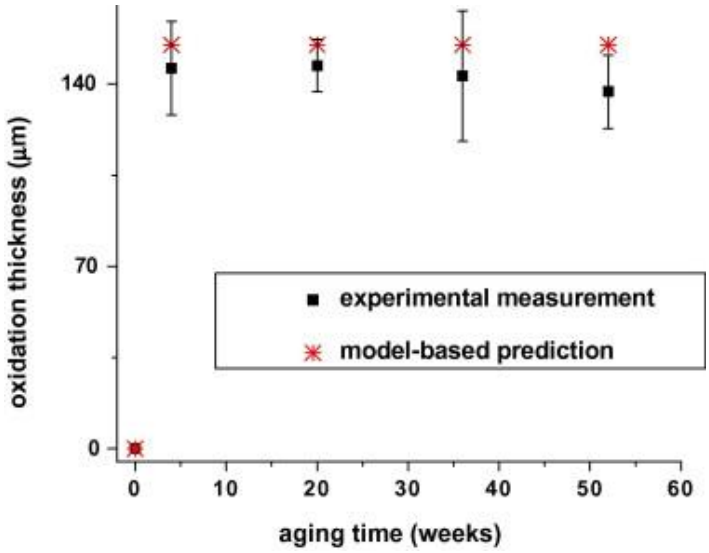

Fig. 8. Experimental measurements and model-based predictions of TOL for different aging time up to 52 weeks at 180 °C.

3.2 Cracking

Aged composite samples were inspected for cracking by preparing transverse and longitudinal polished sections. No evidence of cracking or other forms of damage was detected in the samples that were capped prior to aging, even after aging up to 1 year (8736 h). The surface layer (S_2, shown in Fig. 2), exhibited partial exfoliation of the GFs, limited to 1 or 2 fiber diameters. The matrix in this layer was oxidized and underwent shrinkage, which caused fiber–matrix interface debonding in the near-surface region [18]. The extent of surface exfoliation, which started in the first few weeks of aging, remained unchanged for longer exposures, but exfoliation was more severe at higher exposure temperatures. This outermost surface (S_2), in which fiber orientations were parallel to the surface [16] and [18], inhibited crack initiation and propagation during prolonged exposures.

3.3Mechanical-property retention

The tensile strength of the composite rods remained essentially unchanged after thermal oxidation, as shown in Fig. 10a and b. Small variations in the tensile strength of aged samples were attributed to normal experimental error. In addition, essentially two competing effects affected the strength in the early period of exposure. Additional crosslinking (post-curing) of the matrix caused a slight increase in matrix strength, while aging effects, primarily superficial surface damage from oxidation, caused a slight decrease in composite strength.

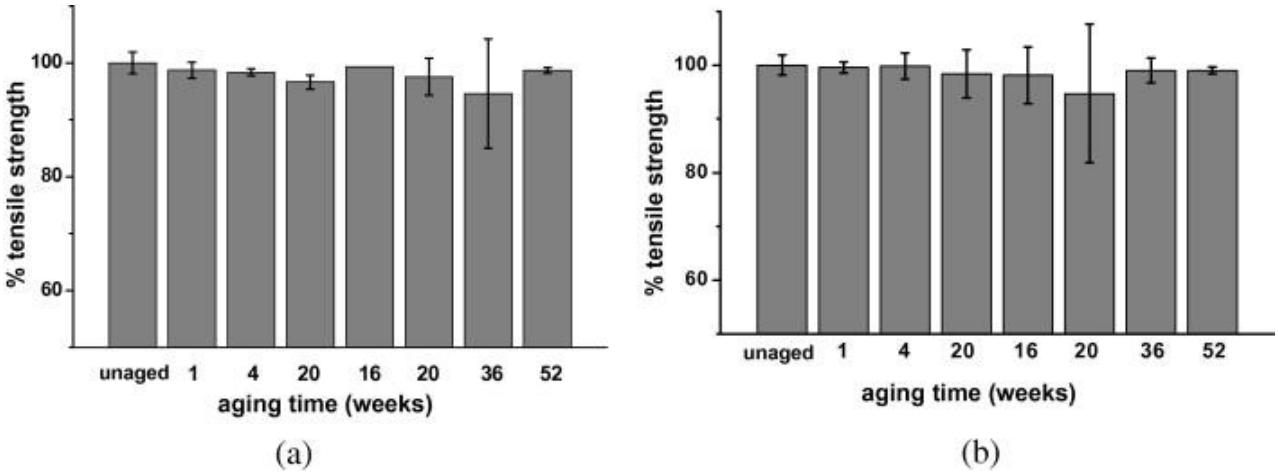

Fig. 10. Tensile strength of the hybrid composite rod exposed at (a) 180 °C and (b) 200 °C in air for 52 weeks.

3.4 Matrix elastic modulus

Matrix oxidation altered the elastic modulus (*E*), particularly within the oxidized layer. Fig. 11 shows the values of the elastic modulus as a function of depth beneath the oxidized sample surface. The values were measured by nanoindentation, and show a clear hardening of the oxidized layer. In addition, the thickness of the oxidized layer (TOL) can be determined from the profile in Fig. 11 [24], and is taken as the depth at which the modulus values reach a constant level. In Fig. 11, the TOL is approximately 110 μm, which is consistent with the results measured from polished sections.

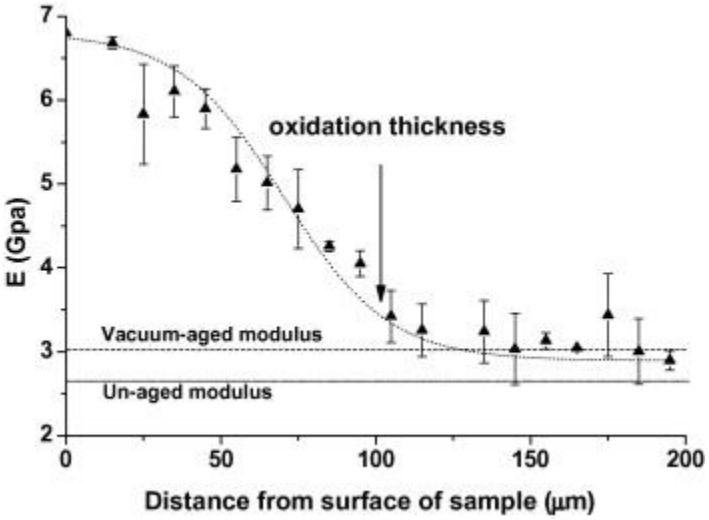

Fig. 11. Elastic modulus as a function of depth for a clear cast polymer sample (3 mm thick) aged for 3200 h at 200 °C

4. Discussion

The GF shell is intended primarily to prevent galvanic coupling between the CF core and the overlaid aluminum wires of the overhead conductor [1] and [25]. However, it also acts as a barrier against oxidization and effectively limits oxidative damage in the hybrid composites to a few fiber diameters. This also prevents oxidative damage of the CF core, which is expected to carry more than 75% of applied loads. While oxygen diffused into the GF shell, penetration was limited to a few fiber diameters because the diffusion was coupled to a reaction. Thus, oxygen never reached the CF/GF interface. Inspection of rods aged for 8736 h showed no evidence of cracks or other damage. The only change observed was exfoliation of 1–2 fiber layers at the GF surface. The exfoliation of fibers can be attributed to structural changes in the matrix and shrinkage associated with the oxidation reaction, which left surface fibers exposed and debonded.

The limited extent of oxidation was supported by measurements and model-based predictions of the TOL for the composite rods, both of which indicated a passivating effect of the oxidized layer. The competition between the rate of oxygen diffusion and the rate of reaction between oxygen and the matrix ultimately determined the TOL. Considering the temperature dependence of diffusion and reaction rates, the ratio of the oxygen-diffusion rate to the oxygen-consumption rate decreased as the temperature increased, and thus the TOL actually decreased with increasing aging temperature [12].

The reaction–diffusion equation presented will provide a valid prediction of the oxygen concentration profile (and the distribution of oxidation products) for a specified aging period, provided the phenomenological model parameters (D, $\boldsymbol{r}_0$, and β) are unchanged during isothermal aging, and no damage occurs to the sample surface. The model parameters change during aging due to oxidation and conversion of the matrix. However, for the conditions studied here, an accurate prediction of oxygen concentration and oxidation product after 1 year of exposure is achieved because of the slow conversion rate of the epoxy matrix. Thus, the model parameters are assumed to be nearly constant over the one-year aging period.

The oxygen concentration profiles provide some guidance for the design of hybrid composites for overhead conductors. The conductor design features a GF shell to protect the CF core from galvanic corrosion, which also limits thermal oxidation. The findings presented here allow one to estimate the required thickness of a GF shell to constitute an effective oxygen barrier. In particular, the TOL was ~150 μm, indicating that a safe design would include a shell substantially thicker than the TOL (depending on desired safety factors and associated risks). Furthermore, the TOL values can be used to estimate the effect on retained tensile strength, as described below.

When a uniaxial load is applied to the composite, the load is shared by the CF, the GF, and the matrix. Assuming elastic behaviour, the tensile strength of the unaged unidirectional composite can be calculated by applying Hooke's law [28].

$$(\delta_C)_F = E_c \cdot (\varepsilon_c)_F = (E\boldsymbol{m} \cdot v\boldsymbol{m} + Egf.vgf + Ecf \cdot vcf) \cdot (\varepsilon_c)_F \quad (17)$$

where the subscripts *c*, *gf*, *cf* and *m* represent the composite, glass-fiber, carbon-fiber, and the matrix, respectively, and $(\delta)_F$ is the tensile strength of the matrix, E is the Young's modulus, ***v*** is the volume fraction, and $(\varepsilon)_F$ is the elongation at break.

Assuming no variations in the GF and CF modulus values after aging, the matrix modulusE_m varies in Eq. (17). Eq. (8) shows that E_m depends on the matrix modulus of the oxidized section, $\bar{E}_{m\text{-}aged}$, and that of the unaged bulk, $E_{m\text{-}unaged}$.

$$E_m = E_{m\text{-}unaged}\, v_{m\text{-}unaged} + \bar{E}_{m\text{-}aged}\, v_{m\text{-}aged} \quad (18)$$

The changes in matrix modulus were confined to the TOL, while the matrix modulus remained unchanged in the bulk of the composite (see Fig. 11). Therefore, the modulus of the aged section is expressed in Eq. (19):

$$\bar{E}_{m\text{-}aged} = \frac{2}{r_o^2 - (r_o - TOL)^2} \int_{r_o - \mathrm{TOL}}^{r_o} r \cdot E_{m\text{-}aged}\, dr \quad (19)$$

where $E_{m\text{-}aged}$ is the local modulus of the aged matrix within the oxidized layer.

Finally, E_m can be expressed by substituting Eq. (19) into Eq. (18):

$$E_m \approx \overline{E}_{m\text{-}unaged}\, v_{m\text{-}unaged} + \frac{2 \cdot v_{m\text{-}aged}}{r_o^2 - (r_o - \mathrm{TOL})^2} \times \int_{r_o - \mathrm{TOL}}^{r_o} r \cdot E_{m\text{-}aged} dr \tag{20}$$

where $\overline{E}_{m\text{-}unaged}$ is the modulus of the vacuum-aged composite. Using the Em-aged values determined from nanoindentation measurements, a sigmoidal curve was fit to the data points (see Fig. 11) in order to calculate the integral in Eq. (20). As a result, the variation in $(E_m)aged$ as expressed in Eq. (20), alters E_c. The ratio of elastic modulus of the aged matrix to that of the unaged matrix is essentially one.

$$\frac{(E_m)_{aged}}{(E_m)_{unaged}} \cong 1.001 \tag{21}$$

Thus, tensile strength is directly proportional to elongation at break, ε_f. In the present study, ε_f was constant for different aging times. The aged cross-sectional area constituted less than 3% of the total cross-sectional area, and had no discernible effect on the failure mode (experimental data showed that ε_f was 1.15 ± 0.05% even after aging for 1 year). Hence, the reduction in composite tensile strength after long-term aging in oxidizing atmospheres is expected to be negligible, an assertion that is supported by the results reported here (Fig. 10).

Sample dimensions can significantly affect the strength retention in oxidizing environments, as shown in Eq. (20). Oxidation thickness is a surface parameter, and thus the TOL remains the same in small-diameter or large-diameter structures. Thus, changes in the composite properties related to TOL are relatively more severe for smaller-diameter rods. For example, for rod diameters less than 1 mm, the volume fraction of aged and unaged sections will be comparable. As a result, for a given

TOL, the ratio of elastic modulus (and ultimate tensile strength) of aged composites to that of unaged composites is not equal to one. Consequently, smaller-diameter structures are expected to be more susceptible to damage from thermal oxidation.

The oxidation process for the hybrid composites studied here is diffusion-controlled, and thus accurate prediction of the TOL using the phenomenological model requires accurate measurement of diffusivity. The diffusion coefficient is not dependent only on the temperature that is expressed by the standard Arrhenius law. Assuming homogenous oxidation for a thin polymer layer, the yield of oxidation (conversion degree) eventually approaches one, indicating that the material structure changes and hence, the transport properties, such as diffusivity, vary over time. In addition, diffusivity is dependent on composition, which varies with distance from the edge of the sample. Therefore, to take into account the effect of diffusivity variation in the phenomenological model, one should measure the diffusion coefficient for different compositions within the TOL. The oxygen diffusivity within the composite matrix was calculated from diffusivity data obtained from the bulk epoxy using a scaling law [16]. However, a difficulty arises in making such measurements because of the brittle (and fragile) nature of thin oxidized polymer films. Our research group has overcome the former problem by developing a method to make uniform thin films of epoxy (<10 μm). Such films are presently being used to perform the requisite diffusivity measurements.

5. Conclusions

A reaction–diffusion model was applied to the thermal oxidation of hybrid GF/CF composites to determine oxygen-concentration profiles and the thickness of the oxidized layer. The predictions

were compared with experimental measurements of oxidized-layer thickness, resulting in an accuracy of >90% for up to a year of thermal exposure. The TOL grew primarily during initial stages, although the growth rate decreased with increasing layer thickness, following parabolic kinetics. The layer did not grow appreciably after four days of exposure, and even exposures of 1 year at 180 °C and 200 °C caused no significant thickening. Thus, the oxidized surface layer effectively functioned as a passive layer, arresting the diffusion of oxygen and protecting the bulk epoxy from further oxidation.

Geometric features of the composite samples significantly influenced the resistance to aging and associated crack initiation. For example, the alignment of fibers parallel to the exposed surface effectively inhibited the advancement of the oxidized layer toward the rod interior. Secondly, no evidence of cracking or other forms of damage was detected during long-term exposures up to 1 year. The crack resistance was attributed to the orientation of high-strength fibers parallel to the exposed surface. Strength retention of similar oxidized composites will depend in part on the ratio of the TOL to the sample diameter. However, the strength loss is expected to be negligible in cases where the ratio of the TOL to the sample diameter is small (<0.1).

An issue of practical importance for overhead conductors concerns the possible effect of thermal aging on long-term durability and retention of mechanical properties. Although the oxidized surface layer reaches a self-limiting thickness and may protect the composite from progressive damage, the surface layer may be disrupted in service by phenomena such as abrasion from overlaid aluminum strands, cyclic bending loads, thermal cycles, and moisture absorption. Repeated disruption of the layer could negate the protective effects and lead to progressive damage. Furthermore, the effects of thermal aging may be more pronounced in small-diameter composite rods, in which the oxidized-

layer thickness constitutes a larger portion of the rod diameter. In addition, tensile loads encountered in service may affect the transport properties of oxygen and reaction-generated volatiles within the composite specimen. Such stress-altered transport properties may well accelerate thermal aging and the associated effects, including microstructural damage.

Acknowledgements: Financial support from Composite Technology Corporation is gratefully acknowledged. The authors also acknowledge Dr. A. Hodge for assistance with nanoindentation experiments.

References:

1. A. Alawar, E.J. Bosze, S.R. Nutt, *A composite core conductor for low sag at high temperatures*, IEEE Trans Power Deliv (2005), p. 20
2. J. Bosze E, A. Alwar, O. Bertschger, Y. Tsai, S.R. Nutt, *High-temperature strength and storage modulus in unidirectional hybrid composites*, Compos Sci Technol, 66 (2006), pp. 1963–1969
3. R. Selzer, K. Friedrich, *Mechanical properties and failure behavior of carbon fibre-reinforced polymer composites under the influence of moisture*, Composite A, 28 (1997), pp. 595–604
4. F. Ellyin, R. Master, *Environmental effects on the mechanical properties of glass-fiber epoxy composite tubular specimens*, Compos Sci Technol, 64 (2004), pp. 1863–1874
5. K. Tsotsis T, *Thermo-oxidative aging of composite materials*, J Compos Mater, 29 (1995), pp. 410–422
6. X. Colin, J. Verdu, *Strategy for studying thermal oxidation of organic matrix composites*, Compos Sci Technol, 65 (2005), pp. 411–419
7. V. Bellenger, J. Decelle, N. Huet, *Aging of a carbon epoxy composite for aeronautic applications*, Composite: Part B, 36 (2005), pp. 189–194
8. T.K. Tsotsis, *Long-term thermo-oxidative aging in composite materials: experimental methods*, J Compos Mater, 58 (1998), pp. 355–368
9. X. Colin, C. Marais, J. Verdu, *Thermal oxidation kinetics for a poly (bismaleimide)*, J Appl Polym Sci, 82 (2001), pp. 3418–3430
10. G.P. Tandon, K.V. Pochiraju, G.A. Schoeppner, *Modeling of oxidative development in pmr-15 resin*, Polym Degrad Stab, 91 (2006), pp. 1861–1869
11. X. Colin, C. Marais, J. Verdu, *A new method for predicting the thermal oxidation of thermoset matrices. Application to an amine crosslinked epoxy*, Polym Test, 20 (2001), pp. 795–803
12. H.M. Le Huy, V. Bellenger, M. Paris, J. Verdu, *Thermal oxidation of anhydride cured epoxies II. depth distribution of oxidation products*, Polym Degrad Stab, 35 (1992), pp. 171–179
13. E. Barjasteh, E.J. Bosze, S.R. Nutt, *Thermal oxidation of anhydride cured epoxy and epoxy matrix composites*, SAMPE Proc, 52 (2008), p. 12
14. J. Decelle, N. Huet, V. Bellenger, *Oxidation induced shrinkage for thermally aged epoxy networks*, Polym Degrad Stab, 81 (2003), pp. 239–248

15. G.A. Schoeppner, G.P. Tandon, E.R. Ripberger, *Anisotropic oxidation and weight loss in pmr-15 composites*, Composites Part A, 38 (2007), pp. 890–904
16. X. Colin, A. Mavel, C. Marais, J. Verdu, *Interaction between cracking and oxidation in organic matrix composites*, J Compos Mater, 39 (2005), pp. 1371–1389
17. T.K. Tsotsis, S.M. Lee, *Long-term thermo-oxidative aging in composite materials: failure mechanisms*, Compos Sci Technol, 58 (1998), pp. 355–368
18. K.J. Bowles, M. Madhukar, D.S. Papadopoulos, L. Inghram, L. McCorkle, *The effects of fiber surface modification and thermal aging on composite toughness and its measurement*, J Compos Mater, 31 (6) (1997), pp. 552–579
19. I.M. Salin, J.C. Seferis, *Anisotropic effects in thermogravimetry of polymeric composites*, J Polym Sci, 31 (1993), pp. 1019–1027
20. K. Kondo, T. Taki, *Moisture diffusivity of unidirectional composites*, J Compos Mater, 16 (1982), pp. 82–93
21. Y.S. Wu, J.V. Vliet, H.W. Frijlink, K.V. Maarschalk, *The determination of relative path length as a measure for tortuosity in compacts using image analysis*, Eur J Pharmaceut Sci, 28 (2006), pp. 433–440
22. G.P. Matthews, M.C. Spearing, *Measurement and modelling of diffusion, porosity and other pore level characteristics of sandstones*, Mar Petrol Geol, 9 (1992), pp. 146–154
23. X. Colin, C.J. Marais, J. Verdu, *Kinetic modelling of the stabilizing effect of carbon fibres on thermal ageing of thermoset matrix composites*, Compos Sci Technol, 65 (2005), pp. 117–127
24. S. Putthanarat, G.P. Tandon, G.A. Schoeppner, *Influence of polishing time on thermo-oxidation characterization of isothermally aged PMR-15 resin*, Polym Degrad Stab, 92 (2007), pp. 2110–2120
25. Boyd J, Chang G, Webb W, Speak S. Galvanic corrosion effects on carbon fiber composites. In: 37th International SAMPE symposium and exhibition: materials working for you in the 21st century, vol. 435; 1992. p. 1184–98.
26. Y.I. Tsai, E.J. Bosze, E. Barjasteh, S.R. Nutt, *Influence of hygrothermal environment on thermal and mechanical properties of carbonfiber/fiber glass composites*, Compos Sci Technol, 69 (2009), pp. 432–437
27. K.D. Ziegel, H.K. Frensdorff, D.E. Blair, *Measurement of hydrogen isotope transport in poly-(vinyl fluoride) films by the permeation-rate method*, J Polym Sci: Part A-2, 7 (1969), pp. 809–819
28. A.K. Kaw, *Mechanics of composite materials*, CRC Press (1997) p. 327